Topics in Catalysis
https://doi.org/10.1007/s11244-022-01752-w

ORIGINAL PAPER

Thermal Sintering and Phosphorus Poisoning of a Layered Diesel Oxidation Catalyst

Miren Agote-Arán[1] · Vilde V. Jacobsen[1] · Martin Elsener[1] · Frank W. Schütze[2] · Christian M. Schilling[2] · Manasa Sridhar[3] · Evangelos Katsaounis[3] · Oliver Kröcher[1,4] · Ivo Alxneit[1] · Davide Ferri[1]

Accepted: 17 November 2022

Abstract
The tightening emission regulations have led to the development of commercial DOCs with zoned or layered formulations allowing to cover a wide range of functionalities (i.e. CO, HC and NO oxidation as well as HC or NOx trap). Aging phenomena in such complex formulations are not well understood. To shed light on material deactivation, this study compares phosphorus poisoning and thermal sintering of two DOC monoliths with related formulations: (1) a commercial monolith comprising two catalytic layers where the top layer is rich in Pt, and (2) a model monolith containing only the top layer of the commercial monolith. The activity and characterisation (elemental analysis, microscopy and N_2-physisorption) results are used to deconvolute the deactivation process of the two layers and should serve to rationalize the aging in layered catalyst formulations.

Keywords Diesel oxidation catalyst · NO oxidation · P poisoning · artificial aging

1 Introduction

A key element for mitigating Diesel vehicle pollution is the Diesel oxidation catalyst (DOC), which is typically located directly after the engine. DOC not only oxidizes CO and hydrocarbons (HC) into inert H_2O and CO_2, but it also converts NO to NO_2. High NO_2 yield is essential for the efficient abatement of NO_x in the selective catalytic reduction catalyst placed downstream as well as for the so-called passive soot oxidation in the particulate filter device, typically directly downstream the DOC [1]. The DOCs come in the form of a catalyst coated on ceramic or metallic monolith substrates [1]. The catalyst contains platinum group metals (PGMs) as the active component and most often consists of Pt-Pd nanoparticles supported on Al_2O_3. While Pt and Pd are both known to be active for CO and HC oxidation, NO oxidation takes place exclusively on metallic Pt [2–5].

According to current emission regulations, heavy duty Diesel vehicles need to be emission compliant for at least 700,000 km [6] and the mileage of compliance is expected to increase in future regulations. Therefore, robustness and stability of the DOC is a crucial requirement and it is of great interest to understand and prevent its deterioration. The DOC suffers from gradual deactivation upon mileage due to thermal and poisoning effects. The catalyst is exposed to high temperatures during fast driving or particulate filter regeneration events that lead to sintering of active PGMs as well as the support. Regarding poisoning, the DOC performance can be compromised by the accumulation of phosphorus (P) and sulphur (S) compounds, which stem from fuel impurities and oil additives such as zinc dialkyldithiophosphates [1, 7–9]. S poisoning results in the sulphation of the PGM particle surface as well as the alumina support [10–12]. With the introduction of ultra-low-sulfur Diesel however, the impact of S poisoning has significantly decreased and P is often the poison present in highest concentration in used catalysts. Deactivation by P is proposed to occur due to reaction with alumina forming phosphate

✉ Miren Agote-Arán
miren.agote-aran@psi.ch

✉ Davide Ferri
davide.ferri@psi.ch

1 Paul Scherrer Institut, 5232 Villigen, Switzerland

2 Umicore AG & Co. KG, D-63457 Hanau-Wolfgang, Germany

3 FPT Motorenforschung AG, CH-9320 Arbon, Switzerland

4 École polytechnique fédérale de Lausanne (EPFL), 1015 Lausanne, Switzerland

Published online: 15 December 2022

species, as well as due to direct coverage of active surface and changes in PGM redox properties [1, 8, 13–18].

An obstacle to fully understand the deactivation phenomena is the fact that thermal aging and poisoning effects overlap [9, 17, 19–24] making it difficult to separate individual and combined aging effects. High temperatures and S exposure for example, are reported to promote PGM sintering [9, 20, 25–29], while the presence of P prevents particle growth [17, 21]. Recent publications reveal that the presence of P also influences the degree of sulphation and modifies the deactivation path [24, 30, 31]. Understanding the aging becomes even more challenging if we consider the evolution of the DOC technology in recent years. The Euro VI regulations approved in 2014 considerably limited the admissible NO_x emissions in Diesel vehicles [6] and much effort has been devoted since to improve the NO_x removal in Diesel aftertreatment systems. Hence, modern DOCs comprise increased Pt content to promote NO oxidation and minimize NO_x emissions; in addition, zeolites are often included to function as "cold traps" to minimize HC emissions during the engine cold start [32–34]. Importantly, a common approach to optimize DOC performance is to deposit multiple washcoats on the monolith creating layers of different composition and functionality [35, 36]. In spite of their commercial relevance, little has been reported on the aging of multilayer catalysts and the rationalization behind the deactivation of different layers is still missing.

On this line, our recent work investigated the aging of a commercial DOC composed of two catalytic layers [24, 31]. Studies on real and artificial aging revealed a stronger deactivation of NO oxidation performance while CO and HC oxidation reactions were less compromised. A hypothesis behind this behavior is that the top layer - Pt rich and with NO oxidation functionality - may be more susceptible to P exposure and thermal aging. To shed some light into the deactivation of commercial DOCs, the present investigation offers an approach towards understanding and separation of the aging phenomena in bilayered catalysts. For this purpose, the individual and combined effects of P poisoning and thermal treatments were evaluated in two monoliths: (1) the commercial DOC formulation comprising two layers (where the top layer is richer in Pt and holds NO oxidation functionality) and (2) a model formulation comprising only the same top layer of the commercial DOC. The comparison of activity and characterisation results after the treatments delivers new insights into the aging phenomena of layered DOC formulations.

2 Experimental

2.1 Materials and Methods

2.1.1 Catalysts

Two full size DOC monoliths (washcoated 400 cpsi cordierite honeycombs) were studied:

a) Commercial DOC (Mc) with a washcoat loading of ca. 100 g L^{-1} (PGM content of 22 g ft^{-3}) and composed of two layers. Both layers contained Pt and Pd as the active elements and Al_2O_3 as the support. The top layer was richer in Pt and NO oxidation to NO_2 is believed to occur exclusively in this layer. The bottom layer also contained a zeolite component providing hydrocarbon storage functionality.
b) Model DOC (Mm), equivalent to the commercial monolith but containing the top catalytic layer only. Hence, the total washcoat loading was half of that of Mc and the precious metal content was ca. 13 g ft^{-3}. Mc and Mm were prepared by the catalyst manufacturing company using the same cordierite, precursors and coating procedures for both samples.

2.1.2 Treatments

Four rectangular segments were extracted (5.0 × 1.2 × 1.7 cm) from the centre of each monolith. To ensure stable catalytic performance, all segments were degreened under a continuous feed of simulated Diesel exhaust (10 vol% O_2, 7 vol% H_2O, 1000 ppm NO, 150 ppm_C1 C_3H_6/C_3H_8 (2:1), 500 ppm CO, balance N_2) at a gas hourly space velocity (GHSV) of 65,000 h^{-1} at 525°C for 4 h. The degreening was performed in the same setup used for activity testing. After degreening, the four segments of each monolith type were subjected to the following treatments:

a) Thermal (labelled as T600 or T750): heating under the simulated Diesel exhaust (GHSV = 65,000 h^{-1}) at 600°C for 20 h or at 750°C for 16 h.
b) Poisoning (labelled as P): by immersing a segment in an aqueous solution of H_3PO_4 (Fluka, 85%) for few seconds followed by drying in static oven at 110°C. The H_3PO_4 concentration in the solution was adjusted to aim for 9.6 wt% P in the coating. The difference in washcoat loading between Mc and Mm was taken into account for the poisoning procedure to ensure equivalent P content in the catalysts. Note that 9.6 wt% in the washcoat corresponds to ~ 1.2 wt% (in Mm) and 2.4 wt% P (in Mc) for the coated catalysts (i.e. cordierite + coating). Considering that previous publications on real aged DOC

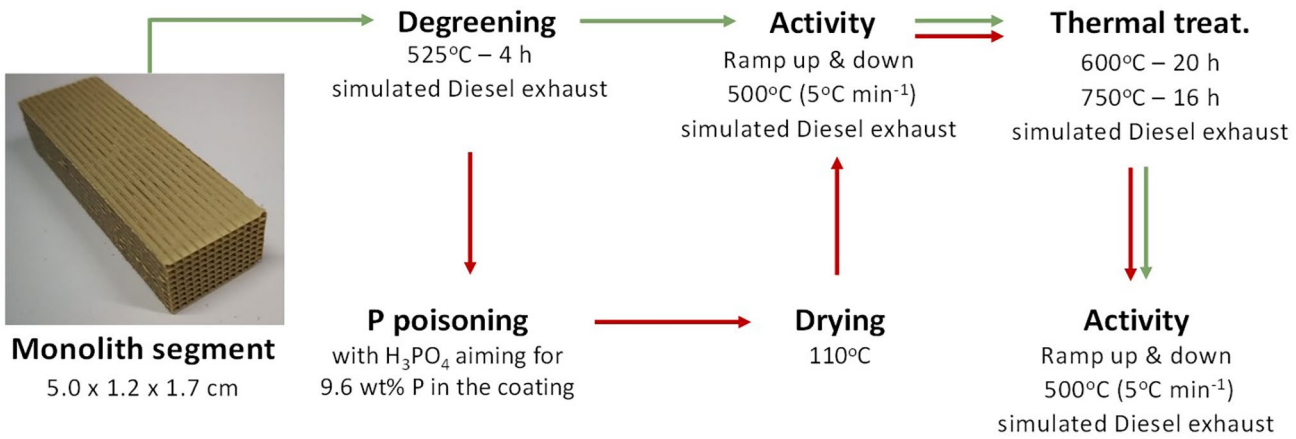

Fig. 1 Schematic representation of the approach followed for treatments of DOC segments

report 0.1–5.3 wt% P in coated catalysts, the used poison content in this study is within the expected range in real application [24, 37].

c) Poisoning and thermal treatment (PT600 or PT750): P poisoning was performed following the procedure described in b); then thermal treatment was performed at 600 or 750°C following the procedure in a).

The resulting samples are denoted by indicating the type of monolith used (Mc or Mm) followed by the treatment performed in such segment (Deg, T600, T750, P, PT600 or PT750). For example, the commercial catalyst segment after P poisoning will be referred to as Mc_P.

2.1.3 Activity Testing

After each treatment, the segments were wrapped with ceramic fibre and placed in a horizontal quartz tube reactor operating at ambient pressure. The outlet gas concentration was analysed using a Fourier transform infrared spectrometer (Nicolet Antaris IGS) equipped with a 2 m gas cell heated to 180°C. The temperature in the reactor was recorded with a thermocouple placed in the sample inlet. All catalytic tests comprised three consecutive heating-cooling cycles under simulated Diesel exhaust at GHSV of 65,000 h^{-1}.

In the first cycle, the binders present in the ceramic fibre were burned off when heating the sample to 500°C at 15°C min^{-1}. After dwelling for 10 min at 500°C, the temperature was decreased to 100°C at the same rate. The pretreatment was followed by two consecutive activity cycles, each performed by heating from 100°C to 500°C and then cooling to 100°C at 5°C min^{-1}. All the results presented in this work correspond to the data collected during the heating ramp of the second activity cycle. The treatment and activity workflow described above is summarised in Fig. 1.

2.2 Characterisation

The elemental composition of the samples was determined by inductively coupled plasma optical emission spectrometry (ICP-OES) using a Varian Vista AX spectrometer. The samples were dissolved using hydrofluoric acid. All calibration solutions were prepared using 99.999% pure chemicals. Nitrogen physisorption measurements were performed at -196°C in a Quantachrome Autosorb-1 instrument. The sample (ca. 150 mg) was outgassed at 350°C overnight under high vacuum prior to the sorption measurements. The Brunauer–Emmett–Teller (BET) equation was applied within the p/p_o range of ca. 0.05–0.30 and used to calculate the specific surface area. The pore size distribution was determined by the Barrett-Joyner-Halenda (BJH) analysis of the isotherm desorption branch. For the scanning electron microscopy and energy dispersive spectroscopy (SEM-EDS) analysis samples were embedded at room temperature in EpoFix resin. The samples were subsequently polished and coated with 10 nm layer of Au in an ion sputter (Leica EM ACE200). The maps were acquired in a ZEISS Ultra-55 Scanning Electron Microscope using an EDAX APOLLO XV Silicon Drift Detector to provide EDS functionality at an accelerating voltage of 12 kV and a working distance of 8.5 mm. For transmission electron microscopy (TEM), the catalyst washcoat was carefully scraped out from the monoliths and finely ground in an agate mortar. The powder was then suspended in ethanol and a drop of the suspension was deposited on a copper grid coated with a holey carbon film. High-angle annular dark-field (HAADF) images were recorded on a FEI Technai F30 FEG scanning transmission

Table 1 Summary of catalytic activity and characterisation results for Mc (commercial) and Mm (model) monolith segments after poisoning and/or thermal treatments

	T20_CO (ºC)		T20_HC (ºC)		Max_NO (%)		SA_{BET} ($m^2 g^{-1}$)		Av. particle size (nm)	
	Mm	**Mc**	**Mm**	**Mc**	**Mm**	**Mc**	**Mm**	**Mc**	**Mm**	**Mc**
Deg	151	154	170	171	62	63	20.3	55.5	5.8	7.2
T600	161	163	178	179	49	48	13.1	56.3	12.7	13.1
P	155	165	183	172	52	50	14.3	42.4	5.6	6.2
PT600	172	156	191	177	46	42	10.9	36.2	8.0	7.5
T750	182	164	198	181	33	35	16.6	47.9	20.4	23.9
PT750	172	164	191	185	34	29	10.4	34.6	8.0	8.5

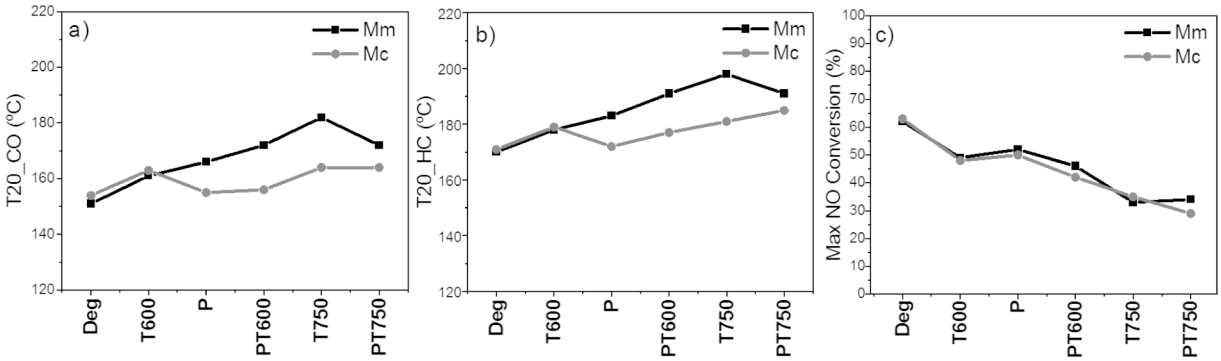

Fig. 2 (a) T20_CO, (b) T20_HC and (c) NO_Max values of Mc and Mm. Sample codes are specified in the text

electron microscope equipped with super twin lens and Schottky type emitter at an accelerating voltage of 300 kV or a probe corrected JEOL ARM200F (NeoARM) equipped with a cold FEG at an acceleration voltage of 200 kV. From the electron micrographs of each sample, the particle size of at least 200 particles were evaluated using the ImageJ software [38]. The particles observed had a close to circular shape, the diameter of such circles was taken as the particle size. Using OriginLab software, the particle diameters were then grouped into evenly spaced bins of 1.5 nm wide. This was defined using the Rice estimator ($n_w = 2n^{1/3}$) and following the work-flow proposed by Alxneit [39].

3 Results and Discussion

The catalytic activity of Mc (commercial bilayered monolith) and Mm (model monolith containing only the Pt-rich top layer) was evaluated by ramping up to 500ºC under simulated Diesel exhaust. The activity was tested after degreening and after each phosphorus and/or thermal treatment (either 600ºC or 750ºC) as shown in Fig. 1. Figure 2 summarises the results by comparing the temperature values at 20% conversion for CO (T20_CO, Fig. 2a) and HC (T20_HC, Fig. 2b) as well as the values for the maximum NO conversion (Max_NO, Fig. 2c). Tabular data of the results can be found in Table 1. While T50 is typically reported to compare catalytic activity, here T20 values are used; the C_3H_6/C_3H_8 mixture 2:1 as HC feed makes T20 a more robust for comparison among samples as indicated in our previous studies [24, 31].

The T20_CO values for Mm_Deg (151°C) and Mc_Deg (154ºC) were very similar. Mm_Deg and Mc_Deg also showed close values of T20_HC (170 and 171ºC, respectively) and Max_NO (60% and 63%). The comparable performance of the two monoliths in the degreened state suggests that the contribution of the top layer dominates the catalytic activity of the bilayer sample. This is expected in views of the higher Pt content in the top layer, which gives this layer with most of the DOC functionality.

The thermal treatment at 600ºC resulted in the deactivation of the DOC performance in both monoliths. This is evidenced by the rise of T20_CO and T20_HC values compared to both Deg references as well as by the decreased Max_NO values. Thus, Mm_T600 and Mc_T600 showed T20_CO of 161ºC and 163ºC respectively, T20_HC values of 178ºC and 179ºC, and Max_NO of 49% and 48%. The similar results obtained for Mc_T600 and Mm_T600 point to an equivalent degree of deactivation in both samples upon the thermal treatment.

On the contrary, the addition of 9.6 wt% P affected Mm and Mc to a different extent. The results in Table 1; Fig. 2

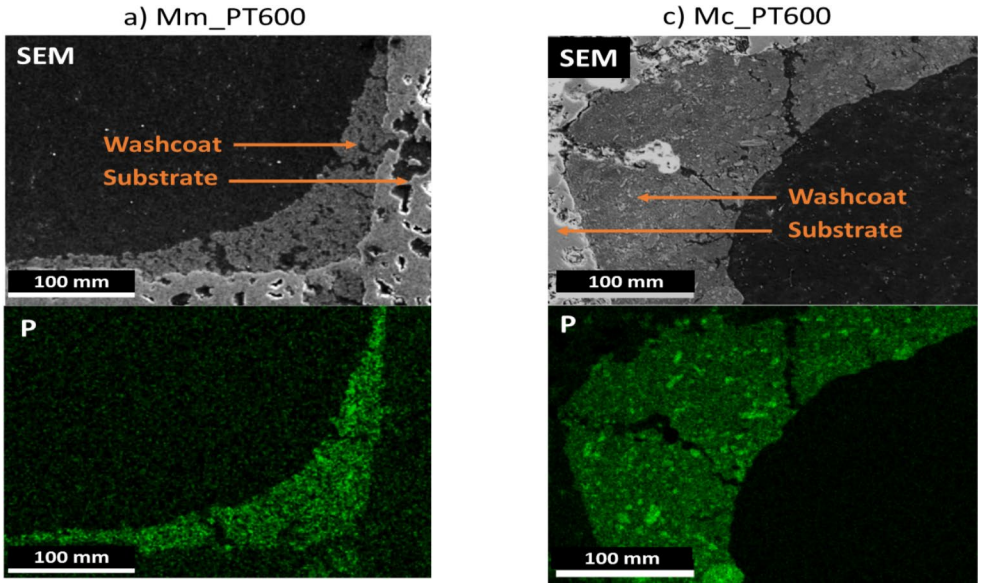

Fig. 3 SEM images and the corresponding EDS element maps for P of cross sections of channel corners (normal to the monolith channels) of (a) Mm_PT600 and (b) Mc_PT600

suggest that P poisoning was more detrimental for CO and HC performance in the one layer sample (i.e. higher T20_CO and T20_HC values for Mm compared to Mc). Nonetheless, very similar NO_max values were obtained in both monoliths indicating similar degree of deactivation in the NO oxidation performance.

Analogous outcome was observed in the subsequent PT600, T750 and PT750 treatments. In all cases, CO and HC oxidation suffered from stronger deactivation of Mm (higher T20_CO and T20_HC values than for Mc) while the impact of the treatments on NO oxidation performance was equivalent in Mc and Mm.

3.1 Characterisation

To confirm that H_3PO_4 treatments led to the aimed poison content, Mm_PT600 and Mc_PT600 were measured by ICP-OES and the results show overall P amounts of 1.2 wt% and 2.4 wt%, respectively. As ICP-OES measurements were conducted with crushed sections, the samples included the cordierite substrate as well as the washcoat. Considering the washcoat loadings on both monoliths, the obtained values translate in P contents of 9.7 wt% (Mm_PT600) and 9.6 wt% (Mc_PT600) in the washcoat of and confirm equivalent levels of poisoning.

The latter calculation works under the assumption that all the P deposits on the catalyst and not on the cordierite. To verify this, the P distribution was evaluated by SEM-EDS. The images in Fig. 3 - corresponding to cross sections of monolith channel corners - illustrate that P was homogeneously distributed in the washcoat in both monoliths. Importantly, it accumulated exclusively in the coating and no poison was found in the cordierite substrate. We have shown previously that formation of aluminium phosphate ($AlPO_4$) is responsible for the diffusion of P through the washcoat [24].

To gain insight into the physicochemical properties of the two monoliths after each treatment the various sections were characterised by N_2 physisorption (surface area, SA_{BET}) and transmission electron microscopy (TEM, PGM particle morphology).

The SA_{BET} values calculated from the N_2 physisorption isotherms are given in Fig. 4a; Table 1. The results reveal that Mc exhibited higher surface areas than Mm; for example, Mc_Deg showed a SA_{BET} value of 55.5 $m^2\ g^{-1}$ while SA_{BET} of Mm_Deg was 20.3 $m^2\ g^{-1}$. The higher surface area of Mc is ascribed to the presence of the microporous zeolite which is a component of the bottom layer. Note that the SA_{BET} was also measured for the sections after crushing in a mortar and thus the analysis comprises the cordierite, which has a low surface area of ca. 5 $m^2\ g^{-1}$. The possible variations of the amount of cordierite present after crushing (typically ca. 75–90 wt%) compromises the accuracy of the analysis. Nonetheless, the general trends in Fig. 4a illustrate that the performed treatments decreased the surface area in Mm and Mc. The drop in SA_{BET} upon thermal and P treatments is ascribed to the sintering of the support material and the formation $AlPO_4$ phases [24, 37, 40]. No sintering is observed for Mc_T600 (SA_{BET} = 56.3 m^2/g) compared to Mc_Deg (SA_{BET} = 55.5 m^2/g), while same treatments lead to sintering in the one layer counterpart (20.3 m^2/g in Mm_Deg and 13.1 m^2/g in McmT600); this suggests that the zeolite - which dominates the surface area in the bilayer catalyst - shows higher thermal stability than the Al_2O_3. The pore blockage as a result of surface area decrease is believed to contribute to DOC deactivation [13], which occurs due to the trapping of active particles (encapsulation) thus preventing them from interaction with the reactants. In case of P

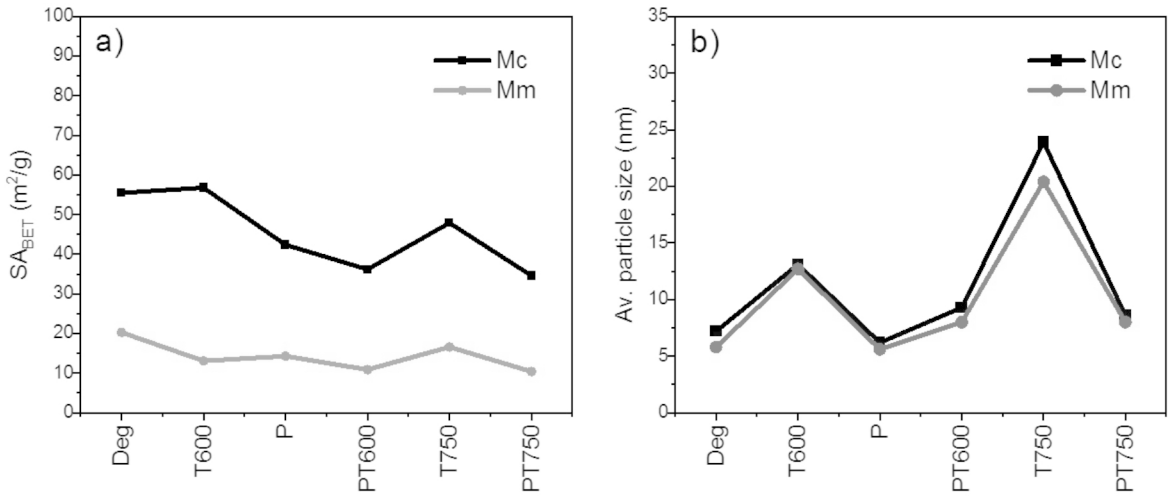

Fig. 4 (a) Specific surface area and (b) average PGM particle size derived from analysis of HAADF-STEM images of Mc and Mm before and after various treatments. Sample codes are specified in the text

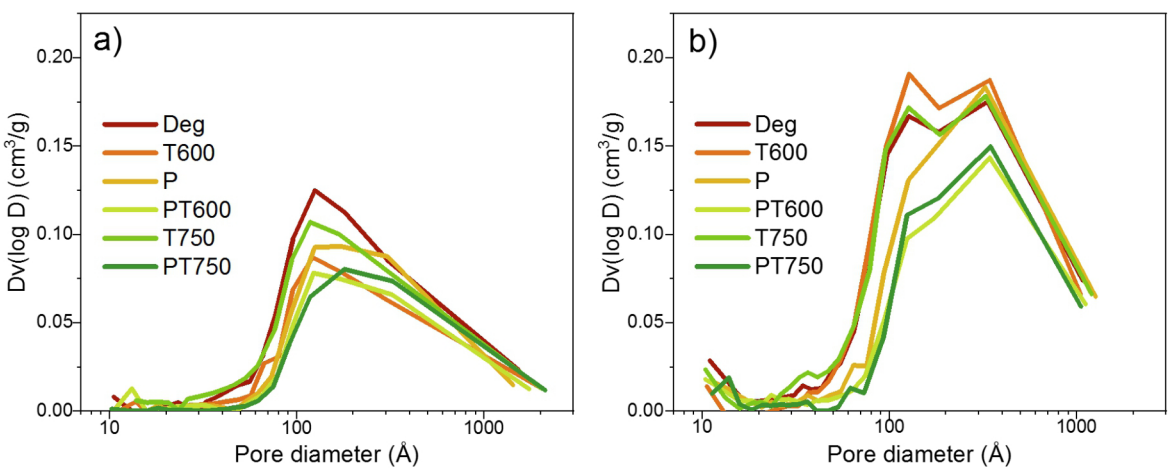

Fig. 5 Pore size distribution of (a) Mm and (b) Mc derived from N_2 physisorption isotherms (BJH method)

poisoning, deactivation can also occur via additional pathways such as direct blockage of the active PGM surface or changes in the redox properties [24].

Barrett-Joyner-Halenda (BJH) analysis of the N_2 desorption branches (Fig. 5) revealed a different pore size distribution of Mc and Mm in the mesopore range (20–500 Å). Mm exhibited pores with average size of ca. 130 Å (Fig. 5a), while Mc presented a bimodal pore size distribution with additional pores with an average diameter of ca. 330 Å. These results enable us to assign the small pores to the top layer and the large pores to the bottom layer present in Mc.

Consistent with SA_{BET}, the pore size distribution plots result in decreased intensity upon P or/and T treatments. Interestingly, the behaviour of the relative intensities of the two types of pores in Mc (Fig. 5b) suggests a more pronounced drop in the fraction of the small pores in response to the P treatment providing evidence for pore blockage by reaction of P with the catalyst and indicating this is more severe in the top layer. This effect can be in part explained by the formulation of the coated layers. Considering the fact that the top layer is composed mainly of Al_2O_3, this support reacts with P leading to $AlPO_4$ formation; in contrast, such reaction should occur to a lower extent in the bottom layer due to the presence of the other components (i.e. zeolite).

The changes in PGM morphology are known to have a strong impact on catalytic activity [1]. The average particle

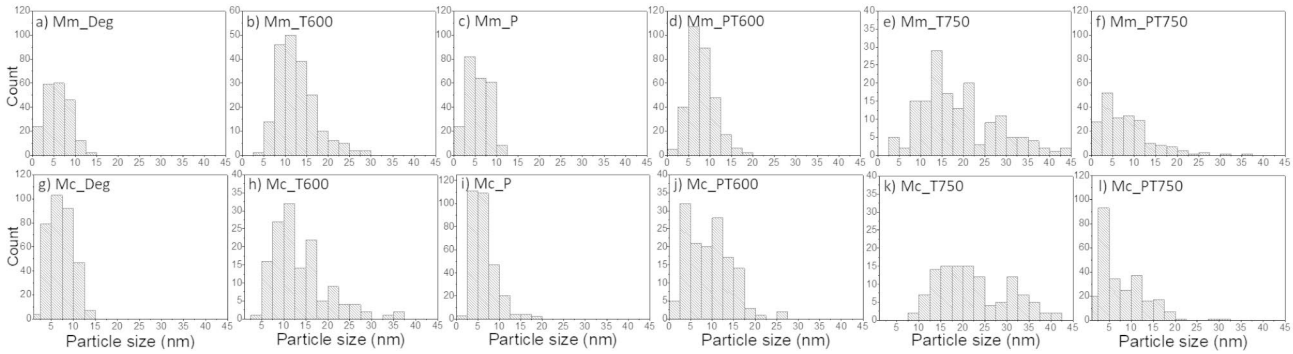

Fig. 6 Distribution of particle sizes obtained for Mm and Mc catalyst in degreened form as well as after each of the phosphorus or/and thermal treatments

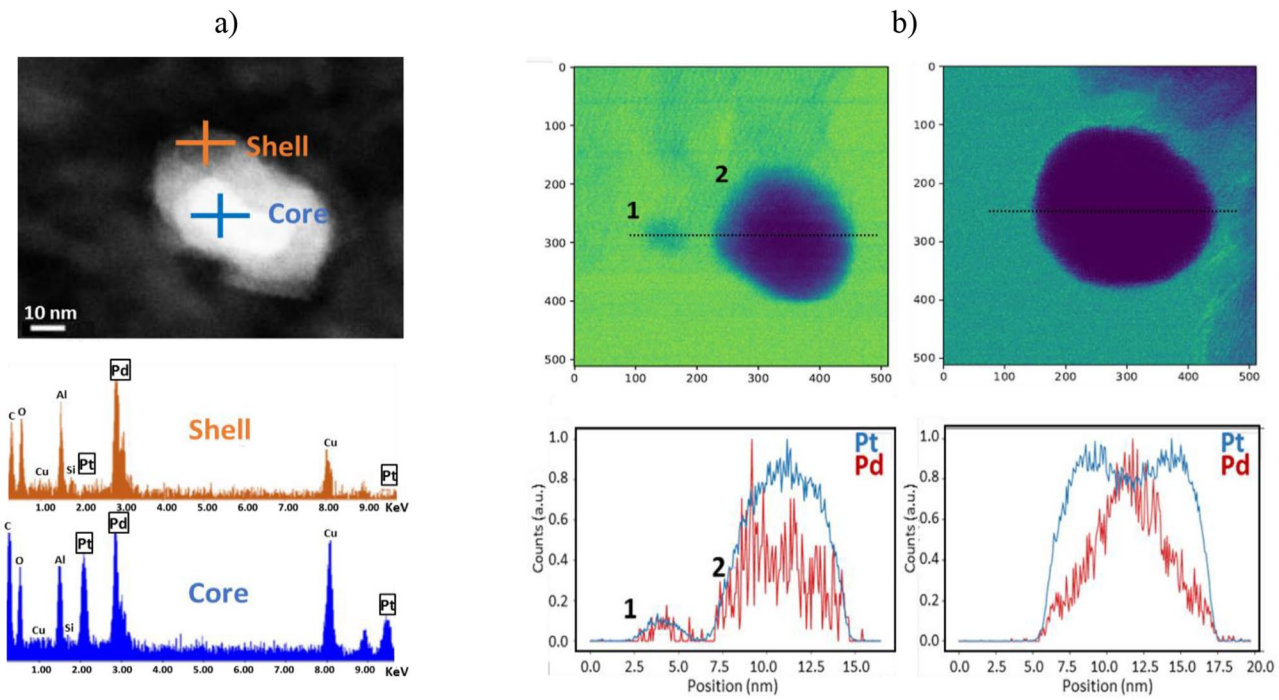

Fig. 7 (a) HAADF-STEM of a selected large PGM particle exhibiting difference in contrast between the core and the shell (top) and the point EDS spectra showing emission from Pd only in the shell, and emission from Pt and Pd in the core; and (b) TEM image of a selected smaller particles (top) and the resulting EDS analysis (bottom) performed along the particle diameter showing normalized Pd (red) and Pt (blue) signals. Si, Al, Cu, O and C signals in panel a correspond to the catalyst support and the copper grid

size of Mm_Deg and Mc_Deg (Fig. 4b; Table 1) obtained from TEM images was 6 and 7 nm, respectively. Both samples exhibited equivalent particle sintering upon thermal treatment at 600ºC resulting in particle growth to ca. 13 nm for both Mm_T600 and Mc_T600. This was also the case after the treatments at 750ºC, which lead to 20 nm and 24 nm particles in Mm_T750 and Mc_T750, respectively. Note that the thermal sintering lead to wide particle size distribution as shown in Fig. 6.

It has been widely observed in the literature that Pt-rich formulations are more prone to thermal sintering while the addition of Pd (to form mixed Pt-Pd particles and alloyed particles) is known to improve the thermal stability of PGM particles [41–43]. The increased stability has been attributed to the formation of a Pd-rich shell, which prevents particle sintering. Our transmission electron microscopy data reveal that such core shell structures are indeed present in Mc. As shown in an example particle in Fig. 7a, large particles exhibit a clear contrast between the particle core (composed of Pt and Pd) and the shell (Pd only) caused by the different distribution of the two elements in the particle. For smaller particles TEM-EDS analysis was performed to evaluate the Pt/Pd ratio across a particle. The results in Fig. 7b suggest that while Pt and Pd enriched domains are present there is

no homogeneous core-shell like distribution among the particles. This is evidenced in examples given with some particles showing a core enrichment with Pt (Fig. 7b left) and others with Pd (right).

Considering the presence of core shell-like structures in the samples and the increased Pt content in the top layer of Mc, a higher degree of PGM sintering was expected in Mm (containing only the Pt-rich top layer) compared to Mc. The equivalent degree of sintering measured in both samples from the average particle size needs to be further assessed as our TEM analysis of Mc did not allow to distinguish particles present in the top layer from those in the bottom layer. Further evaluation of a catalyst containing only the bottom layer would be needed to unequivocally assess the degree of thermal sintering in each layer.

Regarding the effect of poisoning on particle morphology, the P treatment alone (i.e. Mc_P and Mm_P) showed no significant changes compared to the degreened states, and Mc_P and Mm_P exhibited particle sizes of 6 and 7 nm, respectively. The combination of P and thermal (600ºC) treatments resulted in milder sintering than for samples subjected only to thermal treatment; thus, particle sizes of ca. 8 nm were obtained for Mm_PT600 and Mc_PT600. This agrees with previous observations [21, 24] demonstrating that the presence of P prevents the sintering of PGM particles. This can be explained by the particle encapsulation in line with the surface area decrease in Fig. 4a, which hinders PGM mobility and sintering. This appears to apply also to bimetallic Pt-Pd particles as in Mm and Mc catalysts.

Similar conclusions can be drawn from the results obtained from the thermal treatment at 750ºC. As mentioned above, strong sintering of active particles occurred in the absence of P. In contrast, the same treatment but following P poisoning resulted in milder particle growth to only 8 and 9 nm for Mm_PT750 and Mc_PT750, respectively.

Note that the activity results (Fig. 2; Table 1) suggest that P poisoning was detrimental for catalytic performance in all cases, despite the resistance it provided against sintering of the PGMs. We propose that the smaller particle size obtained in P and thermally treated samples results from the encapsulation of particles in the support (via $AlPO_4$ formation [24], pore blockage and subsequent SA_{BET} decrease), which inevitably isolates the active sites from the reactants and compromises the overall catalytic activity. Evidence of encapsulation/coverage is given in our previous studies [24] where we report decreased CO adsorption on PGM particles upon P poisoning. Other deactivation pathways - such as changes in PGM redox dynamics in the presence of P [24] as discussed above - also contribute to the decreased activity of poisoned samples. However, the observation of pore blockage upon P poisoning from the analysis of the pore distribution is a new experimental tile that aids our understanding of catalyst aging.

4 Conclusion

Our previous publications on aging of commercial bilayer DOC showed that this system was particularly susceptible to the deterioration of NO oxidation performance; nevertheless, the role of each catalytic layer and their individual response to aging was unclear. To investigate the behaviour of each coating, P poisoning and/or thermal treatments were performed on two DOC monoliths: (1) the commercial bilayer catalyst (with the top layer richer in Pt), and (2) a model catalyst comprising only the top layer.

The catalytic activity results suggest that all aging treatments are detrimental for the catalytic performance. While the deterioration of NO oxidation activity occurred to equivalent extent in both DOCs, milder deactivation of CO and HC oxidation activity was observed in the bilayer catalyst.

The deactivation upon thermal treatments was attributed to the substantial PGM particle growth observed by TEM. In agreement with previous reports the sintering was minimised when the thermal treatments were accompanied by the presence of P. In spite of the decreased sintering, the addition of P was detrimental for catalytic activity. Based on the selective decrease of a defined size range of pores characteristic of the top layer – richer in Pt and responsible for NO oxidation – we propose that the smaller particle size of consecutively poisoned and thermally treated samples results from PGM encapsulation by the support most likely via formation of $AlPO_4$ and surface area decrease (observed by N_2 physisorption). The deactivation by P poisoning possibly occurs as combination of this encapsulation and else phenomena such as changes in PGM redox properties that we have presented in our previous work.

NO oxidation is expected to occur exclusively in the top layer (Pt rich) and the preferential chemical poisoning of this layer explains the decreased NO oxidation performance upon aging. The higher catalytic activity towards CO and HC oxidation of the two layer DOC (compared to the one layer sample) can be explained by the milder poisoning of the bottom layer which provides CO and HC conversion activity when the top layer is partially deactivated. Hence, the results indicate that a more durable NO oxidation functionality could be achieved by improving the P resistance of the top layer. This can be approached by using a less phosphating support in the top layer, as well as by implementing a P trap upstream of the DOC to minimize the poisoning. We believe that the comparison of multi and single layer catalysts shown in this work helps the rationalisation of aging phenomena in modern DOCs of complex formulation

and sets the basis for improvement of multilayer catalysts for durable NO oxidation performance.

Acknowledgements The authors acknowledge the financial support from the Swiss Innovation Agency (Innosuisse) and are grateful to IAESTE organisation for providing the internship scheme for Vilde V. Jacobsen. Dr. F. Krumeich and Ms. S. Köchli are thanked for the assistance with the TEM and ICP-OES measurements.

Funding Open Access funding provided by Lib4RI – Library for the Research Institutes within the ETH Domain: Eawag, Empa, PSI & WSL.

Declarations

Conflict of Interest The authors declare no competing financial interests.

References

1. Russell A, Epling WS, Catalysis Reviews Science and Engineering Diesel oxidation catalysts (2011) Catal Rev 53:337–423. https://doi.org/10.1080/01614940.2011.596429
2. Morlang A, Neuhausen U, Klementiev KV, Schütze FW, Miehe G, Fuess H, Lox ES (2005) Bimetallic Pt/Pd diesel oxidation catalysts: structural characterisation and catalytic behaviour. Appl Catal B Environ 60:191–199. https://doi.org/10.1016/j.apcatb.2005.03.007
3. Bourges P, Lunati S, Mabilon G (1998) NO_2 fromation during NO reduction on precious metal catalysts. Catal Automot Pollut Control IV 116:213–222. https://doi.org/10.1016/S0167-2991(98)80878-1
4. Deprés J, Elsener M, Koebel M, Kröcher O, Schnyder B, Wokaun A (2004) Catalytic oxidation of nitrogen monoxide over Pt/SiO_2. Appl Catal B Environ 50:73–82. https://doi.org/10.1016/j.apcatb.2003.12.020
5. Kim CH, Schmid M, Schmieg SJ, Tan J, Li W (2011) The effect of Pt-Pd ratio on oxidation catalysts under simulated diesel exhaust. SAE Int 337–343. https://doi.org/10.4271/2011-01-1134
6. https://eur-lex.europa.eu/legal-content/EN/TXT/PDF/?uri=CELEX:02009R0595-20140101&from=EN, (n.d.). https://eur-lex.europa.eu/legal-content/EN/TXT/PDF/?uri=CELEX:02009R0595-20140101&from=EN
7. Kim D, Toops TJ, Nguyen K, Brookshear DW, Lance MJ, Qu J (2020) Impact of lubricant oil additives on the performance of Pd-Based three-way catalysts, Emiss. Control Sci Technol 6:139–150. https://doi.org/10.1007/s40825-019-00138-x
8. Bunting BC, More K, Lewis S, Toops T(2005) Phosphorous poisoning and phosphorous exhaust chemistry with diesel oxidation catalysts, SAE Tech. Pap. 01–1758 329–336. https://doi.org/10.4271/2005-01-1758
9. Andersson J, Antonsson M, Eurenius L, Olsson E, Skoglundh M (2007) Deactivation of diesel oxidation catalysts: vehicle- and synthetic aging correlations. Appl Catal B Environ 72:71–81. https://doi.org/10.1016/j.apcatb.2006.10.011
10. Cabello Galisteo F, Mariscal R, López Granados M, Zafra Poves MD, Fierro JLG, Kröger V, Keiski RL (2007) Reactivation of sulphated Pt/Al_2O_3 catalysts by reductive treatment in the simultaneous oxidation of CO and C_3H_6. Appl Catal B Environ 72:272–281. https://doi.org/10.1016/j.apcatb.2006.11.004
11. Oh S, Kim S, Yoon M, Lee H (2007) Influence of supporting material on the deactivation of diesel exhaust catalysis. React Kinet Mech Catal 90:339–345. https://doi.org/10.1007/s11144-007-5068-6
12. Kolli T, Huuhtanen M, Hallikainen A, Kallinen K, Keiski RL (2009) The effect of sulphur on the activity of Pd/Al_2O_3, Pd/CeO_2 and Pd/ZrO_2 diesel exhaust gas catalysts. Catal Lett 127:49–54. https://doi.org/10.1007/s10562-008-9651-x
13. Neyestanaki AK, Klingstedt F, Salmi T, Murzin DY (2004) Deactivation of postcombustion catalysts, a review. Fuel 83:395–408. https://doi.org/10.1016/j.fuel.2003.09.002
14. Anguita P, García-vargas JM, Gaillard F, Iojoiu E, Gil S, Giroirfendler A (2018) Effect of Na, K, Ca and P-impurities on diesel oxidation catalysts. Chem Eng J 352:333–342. https://doi.org/10.1016/j.cej.2018.07.040
15. Kärkkäinen M, Kolli T, Honkanen M, Heikkinen O, Huuhtanen M, Kallinen K, Lepisto T, Lahtinen J, Vippola M, Keiski RL (2015) The Effect of phosphorus exposure on Diesel oxidation catalysts — part I: activity measurements, Elementary and Surface analyses. Top Catal 58:961–970. https://doi.org/10.1007/s11244-015-0464-z
16. Bergman SL, Granestrand J, Xi S, Du Y, Tang Y, Tang C, Kienkas L, Pettersson LJ, Bernasek SL (2020) Probing the Oxidation/Reduction Dynamics of Fresh and P-, Na-, and K-Contaminated $Pt/Pd/Al_2O_3$ Diesel Oxidation Catalysts by STEM, TPR, and in situ XANES. J Phys Chem C 124:2945–2952. https://doi.org/10.1021/acs.jpcc.9b07655
17. Matam SK, Kondratenko EV, Aguirre MH, Hug P, Rentsch D, Winkler A, Weidenkaff A, Ferri D (2013) The impact of aging environment on the evolution of Al_2O_3 supported Pt nanoparticles and their NO oxidation activity. Appl Catal B Environ 129:214–224
18. Wang A, Wang J, Sheti S, Dahlin S, Han J, Woo J, Xie K, Pettersson LJ, Olsson L (2020) A deactivation mechanism study of phosphorus-poisoned diesel oxidation catalysts: model and supplier catalysts. Catal Sci Technol 10:5602–5617. https://doi.org/10.1039/d0cy00589d
19. Kanerva T, Honkanen M, Kolli T, Heikkinen O, Kallinen K, Saarinen T, Lahtinen J, Olsson E, Keiski RL, Vippola M (2019) Heavy-duty diesel oxidation catalyst and natural gas three-way catalyst. Catalysts 9:137. https://doi.org/10.3390/catal9020137
20. Wiebenga MH, Hwan C, Schmieg SJ, Oh SH, Brown DB, Heui D, Lee J, Peden CHF (2012) Deactivation mechanisms of Pt/Pd-based diesel oxidation catalysts. Top Catal 184:197–204. https://doi.org/10.1016/j.cattod.2011.11.014
21. Winkler A, Ferri D, Aguirre M (2009) The influence of chemical and thermal aging on the catalytic activity of a monolithic diesel oxidation catalyst. Appl Catal B Environ 93:177–184. https://doi.org/10.1016/j.apcatb.2009.09.027
22. Lambert KC, Cheng Y, Dobson D, Hangas J, Jagner M, Hungwen J, Warner J (2009) Post mortem of an aged tier 2 light-duty diesel truck aftertreatment system, SAE Tech. Pap. -01-27. https://doi.org/10.4271/2009-01-2711

23. Lanzerath P, Guethenke A, Massner A, Gaertner U (2009) Analytical investigations on ageing phenomena of catalytic exhaust gas aftertreatment components. Catal Today 147S:S265–S270. https://doi.org/10.1016/j.cattod.2009.07.028
24. Agote-Arán M, Elsener M, Schütze FW, Schilling CM, Katsaounis E, Kröcher O, Ferri D (2021) On the relevance of P poisoning in real-world DOC aging. Appl Catal B Environ 291:1–5. https://doi.org/10.1016/j.apcatb.2021.120062
25. Winkler A, Ferri D, Hauert R (2010) Influence of aging effects on the conversion efficiency of automotive exhaust gas catalysts. Catal Today 155:140–146. https://doi.org/10.1016/j.cattod.2008.11.021
26. Auvray X, Pingel T, Olsson E, Olsson L (2013) The effect gas composition during thermal aging on the dispersion and NO oxidation activity over Pt/Al_2O_3 catalysts. Appl Catal B Environ 129:517–527. https://doi.org/10.1016/j.apcatb.2012.10.002
27. Galisteo FC, Larese C, Mariscal R, Granados ML, Fierro JLG, Fernández-Ruiz R, Furió M (2004) Deactivation on vehicle-aged diesel oxidation catalysts. Top Catal 30/31:451–456. https://doi.org/10.1023/b:toca.0000029789.64784.47
28. Auvray XP, Olsson L (2013) Sulfur dioxide exposure: a way to improve the oxidation catalyst performance. Ind Eng Chem Res 52:14556–14566. https://doi.org/10.1021/ie402153u
29. Olsson L, Karlsson H (2009) The beneficial effect of SO_2 on platinum migration and NO oxidation over pt containing monolith catalysts. Catal Today 147:12–15. https://doi.org/10.1016/j.cattod.2009.07.051
30. Honkanen M, Huuhtanen M, Kärkkäinen M, Kanerva T, Lahtonen K, Väliheikki A, Kallinen K, Keiski RL, Vippola M (2021) Characterization of Pt-based oxidation catalyst - deactivated simultaneously by sulfur and phosphorus. J Catal 397:183–191. https://doi.org/10.1016/j.jcat.2021.03.026
31. Agote-Arán M, Elsener M, Schütze FW, Schilling CM, Sridhar M, Katsaounis E, Kröcher O, Ferri D (2021) Understanding the impact of poison distribution on the performance of Diesel oxidation catalysts. Appl Catal B Environ 299. https://doi.org/10.1016/j.apcatb.2021.120684
32. Westermann A, Azambre B, Finqueneisel G, Da Costa P, Can F (2014) Evolution of unburnt hydrocarbons under "cold-start" conditions from adsorption/desorption to conversion: on the screening of zeolitic materials. Appl Catal B Environ 158–159. https://doi.org/10.1016/j.apcatb.2014.04.005
33. Lee J, Theis JR, Kyriakidou EA (2018) Vehicle emissions trapping materials: successes, challenges, and the path forward. Appl Catal B Environ 243:397–414. https://doi.org/10.1016/j.apcatb.2018.10.069
34. Gu Y, Epling WS (2019) Passive NOx adsorber: an overview of catalyst performance and reaction chemistry. Appl Catal A Gen 570:1–14. https://doi.org/10.1016/j.apcata.2018.10.036
35. Hoke JB, Dettling JC(2016) (12) United States Patent,
36. Chiffey AF, Phillips PR, Moreau F, Daly C, O'Brien M(2015) (12) Patent Application Publication (10) Pub. No.: US 2015/0273452 A1,
37. Rokosz MJ, Lowe-Ma CK, Kucherov AV, Benson D, Paputa Peck MC, McCabe RW (2001) Characterization of phosphorus-poisoned automotive exhaust catalysts. Appl Catal B Environ 33:205–215. https://doi.org/10.1016/S0926-3373(01)00165-5
38. Schindelin J, Arganda-Carreras I, Frise E, Kaynig V, Longair M, Pietzsch T, Preibisch S, Rueden C, Saalfeld S, Schmid B, Tinevez JY, White DJ, Hartenstein V, Eliceiri K, Tomancak P, Cardona A (2012) Fiji: an open-source platform for biological-image analysis. Nat Methods 9:676–682. https://doi.org/10.1038/nmeth.2019
39. Alxneit I (2020) Particle size distributions from Electron Microscopy images: avoiding pitfalls. J Phys Chem A 124:10075–10081. https://doi.org/10.1021/acs.jpca.0c07840
40. Santhosh Kumar M, Otal EH, Aguirre MH, Winkler A, Ulrich A, Rentsch D, Weidenkaff A, Ferri D (2012) Themal and chemical aging of model three-way catalyst Pd/Al_2O_3 and its impact on the conversion of CNG vehicle exhaust. Catal Today 184:237–244. https://doi.org/10.1016/j.cattod.2011.09.030
41. Wilburn MS, Epling WS (2018) A Summary of sulfur deactivation, desorption, and regeneration characteristics of Mono- and bimetallic Pd-Pt methane oxidation catalysts: Pd:Pt mole ratio and particle size dependency, Emiss. Control Sci Technol 4:78–89. https://doi.org/10.1007/s40825-018-0090-x
42. Kaneeda M, Iizuka H, Hiratsuka T, Shinotsuka N, Arai M (2009) Improvement of thermal stability of NO oxidation Pt/Al_2O_3 catalyst by addition of Pd. Appl Catal B Environ 90:564–569. https://doi.org/10.1016/j.apcatb.2009.04.011
43. Ezekoye OK, Drews AR, Jen HW, Kudla RJ, McCabe RW, Sharma M, Howe JY, Allard LF, Graham GW, Pan XQ (2011) Characterization of alumina-supported Pt and Pt-Pd NO oxidation catalysts with advanced electron microscopy. J Catal 280:125–136. https://doi.org/10.1016/j.jcat.2011.03.011